Direct correlation of collagen matrix deformation with focal adhesion dynamics in living corneal fibroblasts

W. Matthew Petroll*, Lisha Ma and James V. Jester

Department of Ophthalmology, University of Texas Southwestern Medical Center, 5323 Harry Hines Blvd. Dallas, TX 75390-9057, USA
*Author for correspondence (e-mail: matthew.petroll@utsouthwestern.edu)

Accepted 7 January 2003
Journal of Cell Science 116, 1481-1491 © 2003 The Company of Biologists Ltd
doi:10.1242/jcs.00357

Summary

The purpose of this study was to develop and apply a new model for investigating how the organization and movement of cell-matrix adhesion sites correlate with force generation by corneal fibroblasts on a fibrillar collagen extracellular matrix. Primary cultures of rabbit corneal fibroblasts were transfected using a vector encoding GFP-zyxin to allow visualization of adhesion sites. Cells were plated at low density on top of 100 μm thick fibrillar collagen lattices embedded with 2 μm diameter red fluorescent beads. Time-lapse imaging was performed at one minute intervals for up to 3 hours. At each time interval, GFP-zyxin, bead and DIC images were acquired in rapid succession using filter wheels. Cells were treated with cytochalasin D and/or Triton X-100 at the end of each experiment. The movements of adhesions and nearby matrix landmarks were measured and correlated from the time-lapse digital images, and the size, intensity and orientation of the adhesions were quantified.

GFP-zyxin was detected in adhesions of transfected corneal fibroblasts as confirmed using vinculin counterstaining. Time-lapse imaging revealed extensions and retractions of cell processes and displacements of the fiduciary beads that were similar to control cells. Extending processes exhibited the most complex behavior, with new adhesions continuously forming at the leading edge while existing adhesions moved backward in a retrograde fashion. This process generated tractional forces as indicated by pulling in of the extracellular matrix in front of the cell. Interestingly, during extension, adhesions along the ventral surface of the cell body generally moved toward those at the tip, resulting in contractile-like shortening and matrix compression at the base of lamellipodia. Overall, a high correlation was found between both the magnitude (R=0.87, *P*<0.001) and direction (R=0.98, *P*<0.001) of the adhesions and nearby matrix displacements. Cytochalasin D induced rapid and reversible disassembly of adhesions, cell elongation and matrix relaxation, including decompression at the base of the lamellipodia. This new experimental model allows direct, dynamic assessment of cell-matrix interactions on a fibrillar collagen matrix. Our results are consistent with the previously described 'frontal towing' model of cell motility and demonstrate for the first time that this mechanism is employed by cells interacting with a fibrillar extracellular matrix.

Movies available online

Key words: Focal adhesions, Focal complexes, Cell motility, Collagen lattice, Actomyosin, Cell mechanics

INTRODUCTION

Cell-matrix mechanical interactions play a defining role in a range of biological processes such as developmental morphogenesis and wound healing. Despite current agreement that fibroblasts exert mechanical forces on the extracellular matrix (ECM) to promote structural organization of the collagen architecture, the underlying mechanisms of force generation and transduction to the ECM are not completely understood. Investigation of these processes has been limited in part by the technical challenges associated with simultaneous imaging of cell activity and measurement of cellular forces.

Early models used to study the mechanical activity of individual fibroblasts were based on the observation that cultured fibroblasts generate compression wrinkles in silicone rubber substrata during locomotion (Harris et al., 1980). On the basis of the pattern of silicon wrinkling, it was proposed that inward directed tractional forces at the leading edge of migrating cells were responsible for extracellular matrix morphogenesis during developmental processes (Harris, 1986; Harris et al., 1981; Stopak and Harris, 1982) as well as wound contraction (Ehrlich, 1988; Ehrlich and Rajaratnam, 1990). A more quantitative model was later developed by attaching the outside edge of the silicon substrata to the inner wall of a chamber, and determining its stiffness using micromanipulation with needles of known rigidity (Lee et al., 1994; Oliver et al., 1995). The forces exerted during cell locomotion could then be estimated from the 2-D displacements of fiduciary beads embedded in the silicon film. More recently, a technique was developed for imprinting a micropattern of dots or lines onto a silicone elastomer, and using them to provide a map of cell-induced deformation of the substrate (Balaban et al., 2001). The regular arrangement of the micropattern provides a more complete force-map than randomly distributed bead markers.

Although all of these experimental models have provided important insights into cell mechanical behavior, they are limited by the fact that silicone is a non-physiological substrate. This limitation has recently been overcome, in part, by the use

of flexible polyacrylamide sheets embedded with fluorescent microspheres as a substratum (Pelham and Wang, 1997; Pelham and Wang, 1999; Wang and Pelham, 1998). Unlike silicone, the surface of these sheets can be coated with ECM proteins, and the material property of the sheet can be controlled by varying the acrylamide/bis-acrylamide ratio. Polyacrylamide sheets have been used to study the magnitude and pattern of force generation during locomotion of normal and H-ras transformed 3T3 fibroblasts (Munevar et al., 2001a), to determine the response of cells to gradients in substrate rigidity (Pelham and Wang, 1997), and to study the effects of myosin inhibitors on the pattern of force generation (Pelham and Wang, 1999).

Recently, the pattern of focal adhesion movement was correlated with tractional force generation on polyacrylamide substrates using fish fin fibroblasts transfected with GFP-zyxin (Beningo et al., 2001). Similarly, the forces generated by focal adhesions in both human foreskin fibroblasts and rat cardiac myocytes transfected with GFP-vinculin were estimated using a micropatterned silicon substrate (Balaban et al., 2001). The ability to directly correlate changes in the organization, movement and turnover of key proteins with the mechanical activity of living cells is a powerful new paradigm that should provide significant advances in the field of cellular mechanics. An important limitation of current models, however, is that cell mechanical interactions on a planar substrate coated with non-fibrillar collagen may be different than that which occurs within a fibrillar extracellular matrix in vivo, since bound, non-fibrillar collagen cannot undergo cell-induced reorganization and remodeling.

In this study, we describe an experimental model for obtaining simultaneous high-resolution time-lapse images of adhesion movement and turnover (using GFP-zyxin) and local ECM deformation by corneal fibroblasts plated on top of fibrillar collagen matrices. This model is more physiologic than models using planar elastic substrates, because fibrillar collagen matrices can undergo cell-induced reorganization and remodeling (Bell et al., 1979; Bellows et al., 1981; Elsdale and Bard, 1972; Grinnell and Lamke, 1984). Furthermore, this model can potentially be applied to study corneal fibroblasts plated inside collagen matrices, which more closely approximates the true 3-D fibrillar ECM with which cells interact in vivo.

Using this new model, we demonstrate that during lamellipodial extension, new adhesions form in association with membrane ruffling at the leading edge while existing adhesions move backward centripetally in a retrograde fashion. This process generates tractional forces as indicated by pulling in of the ECM in front of the cell. Interestingly, during extension, cell body adhesions moved in the opposite direction to those in the lamellipodia, compressing the ECM at the base of the lamellipodia. Cytochalasin D induced rapid and reversible disassembly of adhesions, cell elongation and ECM relaxation. Overall, the data provide important new evidence that supports and extends the previously described ‘frontal towing’ model of cell motility (Munevar et al., 2001a), and demonstrate for the first time that this mechanism is employed by cells interacting with a fibrillar ECM.

Materials and methods

Cells

Corneal fibroblasts were harvested from New Zealand White Albino rabbit eyes (Pel-Freez, Rogers, AR). The eyes were washed 2 times with RPMI (Gibco BRL, NY) supplemented with 1% penicillin and 1% streptomycin (Biowhittaker, Wakersville, MD). The epithelium was removed by scraping with a surgical blade and swabbing with alcohol pads. Corneal buttons were dissected with care taken not to include any scleral tissue. The monolayer of endothelium was removed by swabbing with sterile cotton-tipped applicators dipped in 70% ethanol solution. Corneas were digested overnight in a 37°C incubator with 2 mg/ml collagenase and 0.5 mg/ml hyaluronidase solution. Fibroblasts were washed 2 times and cultured in 25 cm tissue culture flasks (Costar, Cambridge, MA) using ‘complete media’ consisting of modified Eagle minimal essential media (MEM; Sigma, St. Louis, MO) supplemented with 1% penicillin, 1% streptomycin and 1% fungizome (Biowhittaker, Wakersville, MD) and 10% fetal bovine serum (FBS; Sigma), and incubated at 37°C in a humid atmosphere containing 5% CO_2.

Transfection

For expression of GFP-zyxin, human zyxin in a pEGFP-N1 vector (Clontech laboratories, Palo Alto, CA) was used. This probe was a generous gift of Professor J. Wehland and coworkers (BGF, Braunschweig, Germany), and has been used previously as a marker for focal contacts in goldfish fin fibroblasts (Beningo et al., 2001; Kaverina et al., 2000; Kaverina et al., 1999) and mouse melanoma cells (Rottner et al., 2001). The unmodified pEGFP-N1 expression vector was used as a control. Only first or second passage corneal fibroblasts were used for transfections, since we have found previously that cell mechanical activity is reduced after multiple passages. Corneal fibroblasts were plated on six-well plates (40,000 cells/well) using complete media without antibiotics 24 hours before transfection. Transfection was performed using Lipofectamine PLUS (Invitrogen, Carlsbad, CA). For each well, 0.5 μg of GFP-zyxin DNA in 100 μl DMEM was pre-complexed with 3 μl PLUS reagent for 15 minutes. Meanwhile, 2.5 μl Lipofectamine reagent was mixed with 100 μl DMEM. Pre-complexed DNA and diluted Lipofectamine reagent then were mixed and incubated for 15 minutes at room temperature. Cells were then incubated with DNA-PLUS-Lipofectamine reagent complex mixed with an additional 800 μl of DMEM (total of 1 ml of media per well). After 3 hours of incubation at 37°C (5% CO_2), 1 ml of DMEM and 20% FBS was added to each well. After 24 hours, transfection media was replaced with complete media.

Collagen matrices

Hydrated collagen matrices were prepared by mixing neutralized bovine dermal collagen (Vitrogen 100; Collagen Corporation, Palo Alto, CA) with 10× MEM to achieve a final collagen concentration of 2.48 mg/ml. The collagen solution was kept on ice at all times. Carboxylate-modified red fluorescent latex beads (2.0 μm diameter; Molecular Probes, Eugene, OR), suspended in MEM supplemented with 1% penicillin and 1% streptomycin, were briefly sonicated (Sonabox, Model 300; Fisher, Pittsburgh, PA) to prevent agglomeration of the latex particles prior to mixing with the collagen solution at 1:10 (v/v) ratio. The pH of the collagen solution was adjusted to 7.2-7.4 by addition of 0.1 N NaOH or 0.1 N HCl.

For plating cells on top of the lattice, 30 μl aliquots of the collagen/bead mixture were poured onto Delta T glass bottom culture dishes (Bioptechs, Butler, PA) and polymerized for 60 minutes at 37°C. Each aliquot was spread over a central 10 mm diameter circular region on the dish. This resulted in gels approximately 100 μm thick after polymerization. GFP-zyxin transfected or control (pEGFP-N1 transfected or untransfected) corneal fibroblasts were harvested with 0.05% trypsin/0.53 mM EDTA at 37°C for 2 minutes. The cells were washed 2 times with complete media and then diluted to a final concentration of 10^4 cells/ml. One hundred μl of cell suspension

(1000 cells) was seeded on top of the matrix and placed in a humidified incubator (37°C, 5% CO_2) for 30 minutes to promote cell attachment. The matrix was then overlaid with 2 ml of complete media. The matrices with cells were then incubated overnight prior to time-lapse imaging.

Immunofluorescence staining

In order to confirm that GFP-zyxin was being organized into cell-matrix adhesions, cells were counter-stained for vinculin and F-actin. For staining, cells were plated directly onto Delta T dishes. After 18 hours, cells were fixed using 1% paraformaldehyde in phosphate buffer for 3 minutes, permeabilized in acetone at –20°C for 5 minutes, and rehydrated in phosphate buffer. For vinculin staining, nonspecific staining was blocked by incubation with 0.1 mg/ml whole goat serum (Organon Teknika, Durham, NC) for 30 minutes. The serum was removed and cells were incubated for 1 hour in mouse monoclonal antibody to human vinculin (Clone V284, dilution 1:100; Serotic, Washington, DC). Cells were then washed in buffer and incubated for 1 hour in affinity-purified rhodamine conjugated goat anti-mouse IgG (dilution 1:20; ICN Biomedicals, Aurora, OH). For F-actin labeling, cells were incubated in rhodamine phalloidin (dilution 1:20; Molecular Probes, Eugene, OR) for 30 minutes following permeabilization. Fluorescent microscopy and digital imaging was performed using the Nikon system described below.

Time-lapse digital imaging

Microscopy was performed using a Nikon TE300 inverted microscope with fluorescence and differential interference contrast (DIC) imaging modules (Nikon, Melville, NY), two high speed filter wheels for rapid selection of excitation and emission filters and shuttering of epifluorescent illumination (Lambda 10-2, Sutter Instruments Company, Novato, CA), a transmitted light shutter (Uniblitz, Vincent Associates, Rochester, NY) and a high resolution cooled CCD camera (CoolSnap HQ, Roper Scientific, Tuscan, AZ). The hardware was controlled using a PC running MetaView (Universal Imaging, Downingtown, PA). To maintain cell viability during imaging, a Bioptechs microincubation system and objective heater was used (Bioptechs, Butler, PA). With the Bioptechs system, cells can be both cultured and imaged in special dishes with glass bottoms the thickness of #1 cover slip (~0.17 mm); this increases the free working distance as compared with plastic and is also compatible with DIC imaging. Cells were continuously perfused while on the microscope stage with complete media containing 50 mM HEPES buffer at a rate of 6 ml/hour using a Bioptechs microperfusion pump.

In each experiment, the activity of a single cell was imaged for up to 3 hours using a 60× oil immersion objective (1.3 NA, 220 μm free working distance). Cells were imaged approximately 18 hours after seeding on the gel; this allowed them to develop a more consistent bipolar spindle-shaped morphology as is observed during in vivo wound healing (Cukierman et al., 2001; Moller-Pedersen et al., 1998a; Moller-Pedersen et al., 1998b; Petroll et al., 1993). Images were automatically acquired at 1 minute intervals using MetaView. At each time point three images were acquired in rapid succession: one using bandpass FITC excitation and emission filters (for EGFP), one using Propidium Iodide (PI) excitation and emission filters (for red fluorescent beads), and one using DIC. A DAPI/FITC/PI beam splitter was used for all acquisitions (Chroma Technology, Brattleboro, VT). To minimize phototoxicity and photobleaching, neutral density filters were used and exposure times were kept to a minimum by using 2×2 on-chip camera binning. With binning, the images were 696×520 pixels. Typical camera exposure times for each GFP, bead and DIC image were 1 second, 2 mseconds and 250 mseconds, respectively.

In a subset of five experiments, the perfusion was stopped after 2-3 hours and cytochalasin D (Sigma) was added to the culture dish (final concentration 25 μM) in order to assess the effect of F-actin on cellular force generation. After 15-20 minutes, the perfusion was restarted in two experiments to assess the reversibility of this effect. Cells were lysed using 1% Triton X-100 (Sigma) at the end of every experiment to assess cell-induced matrix deformation.

Analysis of matrix deformation

In order to map the ECM deformation, the red fluorescent beads were tracked using the 'object tracking' module in MetaMorph (Universal Imaging, Downingtown, PA). Beads in the first PI image of the temporal sequence were manually marked and used as seed points. The centroid for each of the beads was then automatically determined, and used as the seed point for the next image in the temporal sequence. The template matching option was found to work best for bead tracking. This procedure uses a cross correlation routine to identify corresponding beads in each sequential image. For each image in the time-lapse sequence, the x,y coordinates of the bead centroids were automatically logged into an Excel file (Microsoft, Redmond, WA) for later analysis.

We observed that the organization of the collagen matrix could be clearly visualized using high magnification DIC imaging. Thus we investigated whether MetaMorph could be used to track ECM deformation directly from the DIC images (i.e. without using beads). We found that the 'threshold result' algorithm within the MetaMorph object tracking routine worked best for this application. Preprocessing included the 'flatten background' and 'equalize stack' procedures that allowed a single threshold to be used for the entire time-lapse sequence. After thresholding, landmarks in the first DIC image of the temporal sequence were manually marked and used as seed points. The automated tracking was then performed as described above, except that the centroid for each landmark was determined using above-threshold pixels within a small window surrounding each seed point. To verify that our ECM tracking algorithm was correctly mapping ECM deformation, we compared the magnitude and direction of ECM displacements with nearby beads using linear regression analysis.

Assessment of adhesion organization

In order to measure the size, orientation, intensity, and location of adhesions over time, we used the Integrated Morphometry Analysis (IMA) feature of MetaMorph. Preprocessing included the 'flatten background' and 'equalize stack' procedures that allowed a single threshold to be used for the entire time-lapse sequence. The location, intensity and morphometry of each above-threshold adhesion could then be recorded for each frame in the sequence using IMA.

Color overlays

Color overlay images of GFP-zyxin (in green) and fiduciary beads (in red) were generated using the 'Overlay Images' feature in MetaMorph. In order to display the bead, ECM and adhesions tracks, a custom program was developed using Visual Basic (Microsoft, Redmond, WA). This program read the coordinates from the Excel file and drew the path of each tracked object onto a sequence of images. The tracks could then be overlaid onto other image sequences as needed, using MetaMorph.

Results

Vinculin and F-actin counterstaining

In order to determine whether GFP-zyxin was being properly organized into cell-matrix adhesion sites, cells were counterstained for vinculin and F-actin. GFP-zyxin (green) and vinculin (red) were co-localized into punctate spots (yellow) in the lamellipodia, as well as larger, more elongated structures

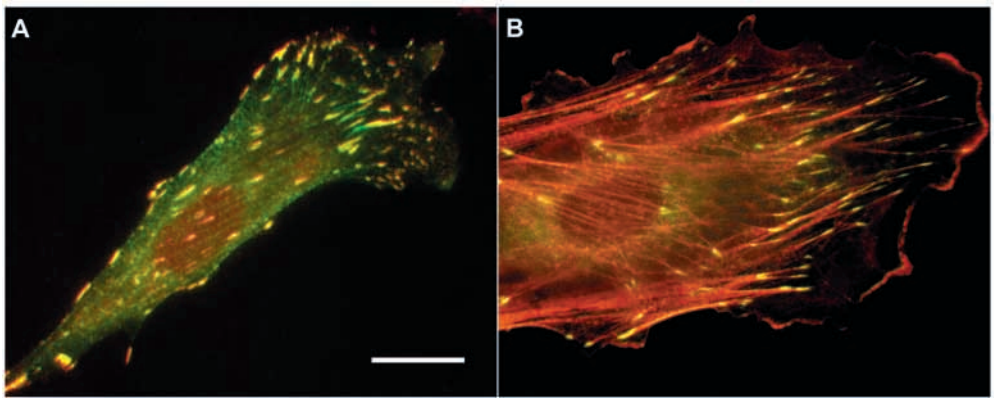

Fig. 1. Corneal fibroblasts transfected to express GFP-zyxin were plated on glass dishes and labeled for (A) vinculin and (B) F-actin organization. (A) GFP-zyxin (green) and vinculin (red) were co-localized into punctate spots (yellow) in the lamellipodia, as well as larger, more elongated structures along the cell body. (B) Yellow spots demonstrate that GFP-zyxin (green) is localized to the ends of the F-actin stress fibers (red), which is the expected localization of focal adhesions. Weaker GFP-zyxin labeling in a periodic pattern along the stress fibers is also observed. Bar, 20 μm.

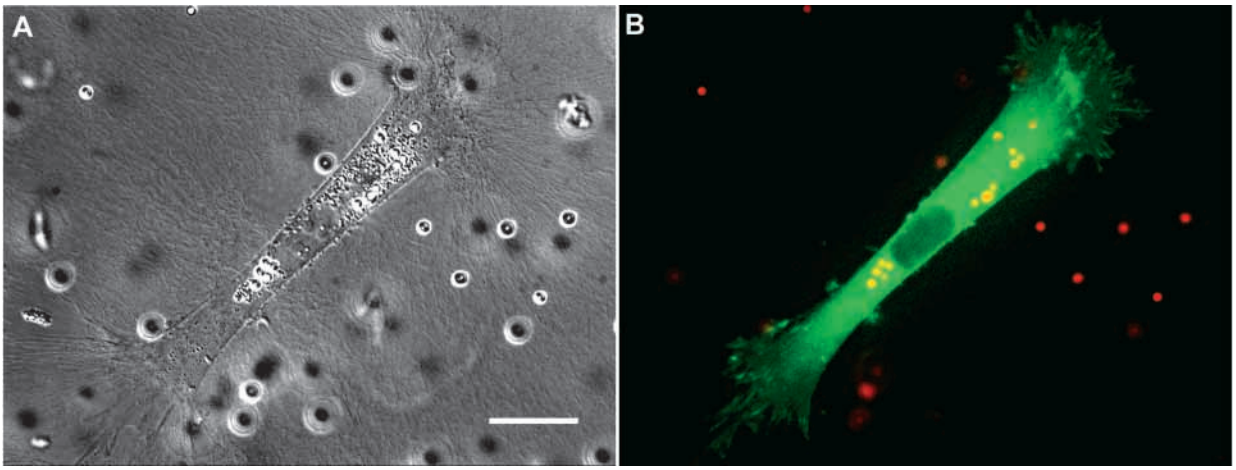

Fig. 2. DIC and fluorescent color overlay images of living corneal fibroblast expressing GFP-zyxin, 18 hours after plating on top of a fibrillar collagen matrix. (A) DIC imaging allowed detailed visualization of the fibrillar collagen organization in addition to the beads. (B) GFP-zyxin (green) was organized into adhesions that were most concentrated at the leading edge (upper right) and tail of the cell. Adhesions at the leading edge were generally organized into a radial pattern. Diffuse background GFP-zyxin labeling was also observed. Fiduciary beads are also visible (red). Bar, 20 μm. See also movie 1 at jcs.biologist.org/supplemental.

along the cell body (Fig. 1A). This is the expected labeling pattern for focal complexes and focal adhesions, respectively (Rottner et al., 1999). Fig. 1B allows comparison of F-actin (red) and GFP-zyxin (green). Notice that the strongest zyxin labeling is localized to the ends of the F-actin stress fibers, which is the expected localization of focal adhesions. Weaker labeling in a periodic pattern along the stress fibers is also observed, consistent with zyxin organization in other cell types (Rottner et al., 2001). A similar cellular morphology and pattern of vinculin and phalloidin labeling was observed in untransfected cells (not shown).

Time-lapse imaging: general observations

Eighteen hours after plating on the gel, most cells (both GFP-zyxin transfected and controls) had a bipolar morphology similar to in vivo wound healing corneal fibroblasts. The cell density was sparse enough to focus on the mechanical activity of isolated cells. DIC imaging allowed detailed visualization of the fibrillar collagen organization in addition to the beads and cells (Fig. 2A). GFP-zyxin was organized into adhesions that were most concentrated at the leading edge and tail of the cell (Fig. 2B), although adhesions were also present along the ventral surface of the cell body. In general, these adhesions were slightly below those at the ends of the cell, and thus were not always visualized in the same focal plane. Adhesions at the leading edge were generally organized into a radial pattern. Diffuse background GFP-zyxin labeling was also present, suggesting a cytoplasmic pool of this protein. Control cells transfected with the EGFP-N1 vector alone had bright and diffuse non-specific cytoplasmic and nuclear labeling, with no specific labeling of adhesions (not shown).

Fibroblast migration was characterized by lamellipodial extension at the leading edge, forward movement of the cell body, and small intermittent retractions of the rear of the cell. After 30-60 minutes of directional migration, the cells would sometimes change their direction of movement. This most often occurred after a large retraction at the rear of the cell.

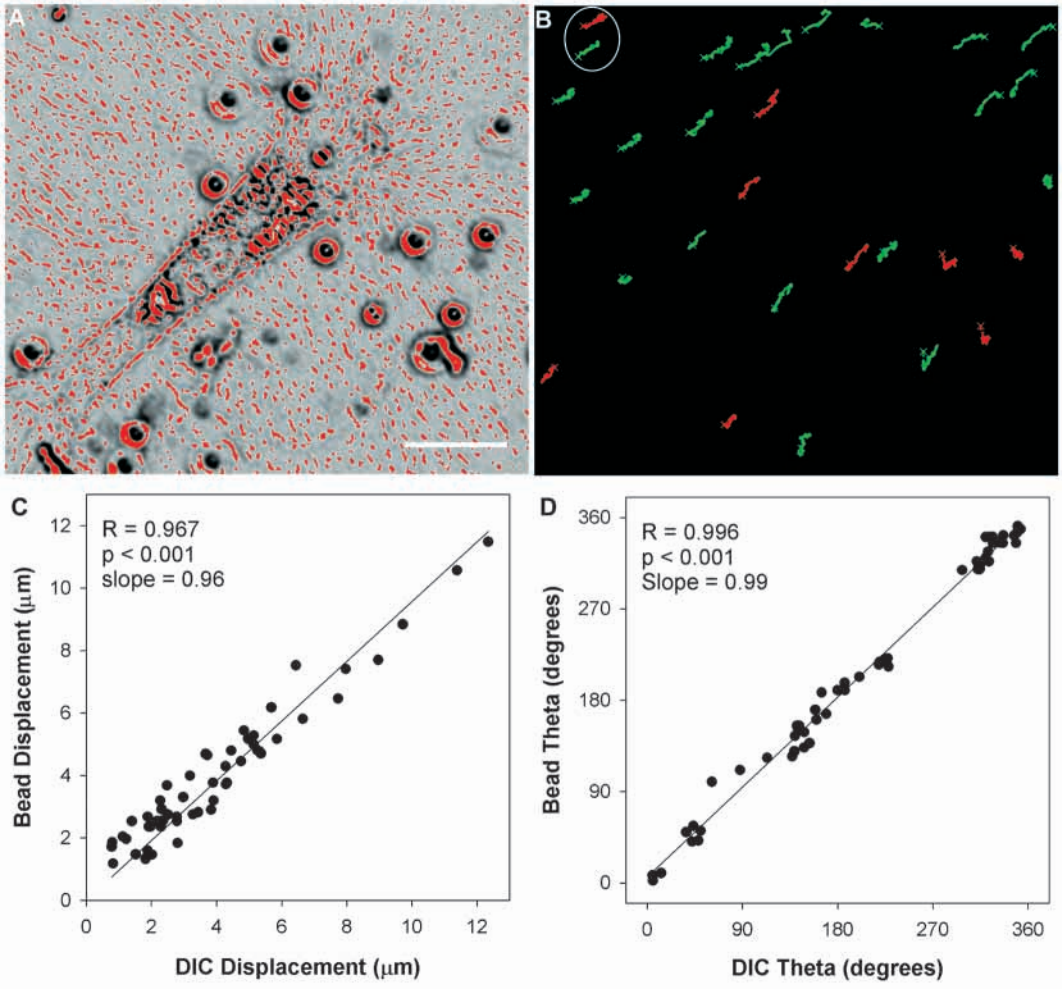

Fig. 3. Investigation into whether the ECM deformation could be measured directly from DIC images. (A) A segmented DIC image. Above-threshold (red) spots were used as ECM landmarks and tracked over time. (B) Color overlays of bead (red) and DIC (green) tracks (cross indicates initial position in the sequence). Tracks that are close to each other show the same pattern of movement (circle). (C,D) The magnitude and direction of selected bead and DIC tracks taken from five experiments were analyzed. A high correlation was found between both the (C) magnitude and (D) direction of the bead and DIC displacements. Bar, 20 μm.

Thus, consistent with previous studies, a slow random walk pattern of migration was achieved (Roy et al., 1999b). Using DIC imaging, membrane ruffling during lamellipodial extension was clearly observed at the leading edge. During extension, new adhesions formed when the ruffling membrane 'touched down' on the ECM at the leading edge; meanwhile, existing adhesions move backward centripetally in a retrograde fashion and eventually disappeared (Movie 1, available at jcs.biologists.org/supplemental). This process generated tractional forces as indicated by pulling in of the ECM in front of the cell. In most cells, there was a cycle of membrane ruffling and new adhesion formation that repeated itself as the cell moved forward. The same pattern of membrane ruffling and ECM deformation was observed in both EGFP-N1 transfected and untransfected control cells (not shown).

Direct tracking of collagen ECM deformation

Fiduciary beads have been used previously to map ECM deformation on both planar elastic substrates and collagen matrices (Lee et al., 1994; Oliver et al., 1995; Pelham and Wang, 1999). We used this approach in earlier studies in which low magnification (20× or 32×) phase contrast imaging was used (Roy et al., 1997; Roy et al., 1999a; Roy et al., 1999b). However, since the organization of the collagen matrix could be more clearly visualized using high magnification DIC imaging, we investigated whether the ECM deformation could be measured directly from the DIC images (i.e. without using beads). We first developed a procedure for segmenting the DIC image so that ECM landmarks could be tracked (Fig. 3A). We then generated color overlays of the bead (red) and DIC (green) tracks so that their pattern of movement could be compared (Fig. 3B). It was apparent from these overlays that they were highly correlated. However, to demonstrate this quantitatively, the magnitude and direction of selected bead and DIC tracks taken from five experiments were analyzed. The analysis was performed using bead and DIC tracks that were close to each other (Fig. 3B, circle), and not within 20 μm of a cell, since ECM deformations near the cell can vary substantially over short distances. A high correlation was found between both the magnitude ($R=0.967$, $P<0.001$; Fig. 3C) and direction ($R=0.996$, $P<0.001$; Fig. 3D) of the bead and DIC displacements. On the basis of this finding, we used both bead and DIC tracks to map ECM deformation throughout this study.

Analysis of adhesion dynamics

Tracking of adhesion movement was performed using a semi-automated procedure in MetaMorph, in which above-threshold adhesions in each frame were selected manually, and their location (centroid), size, orientation and pixel intensity were

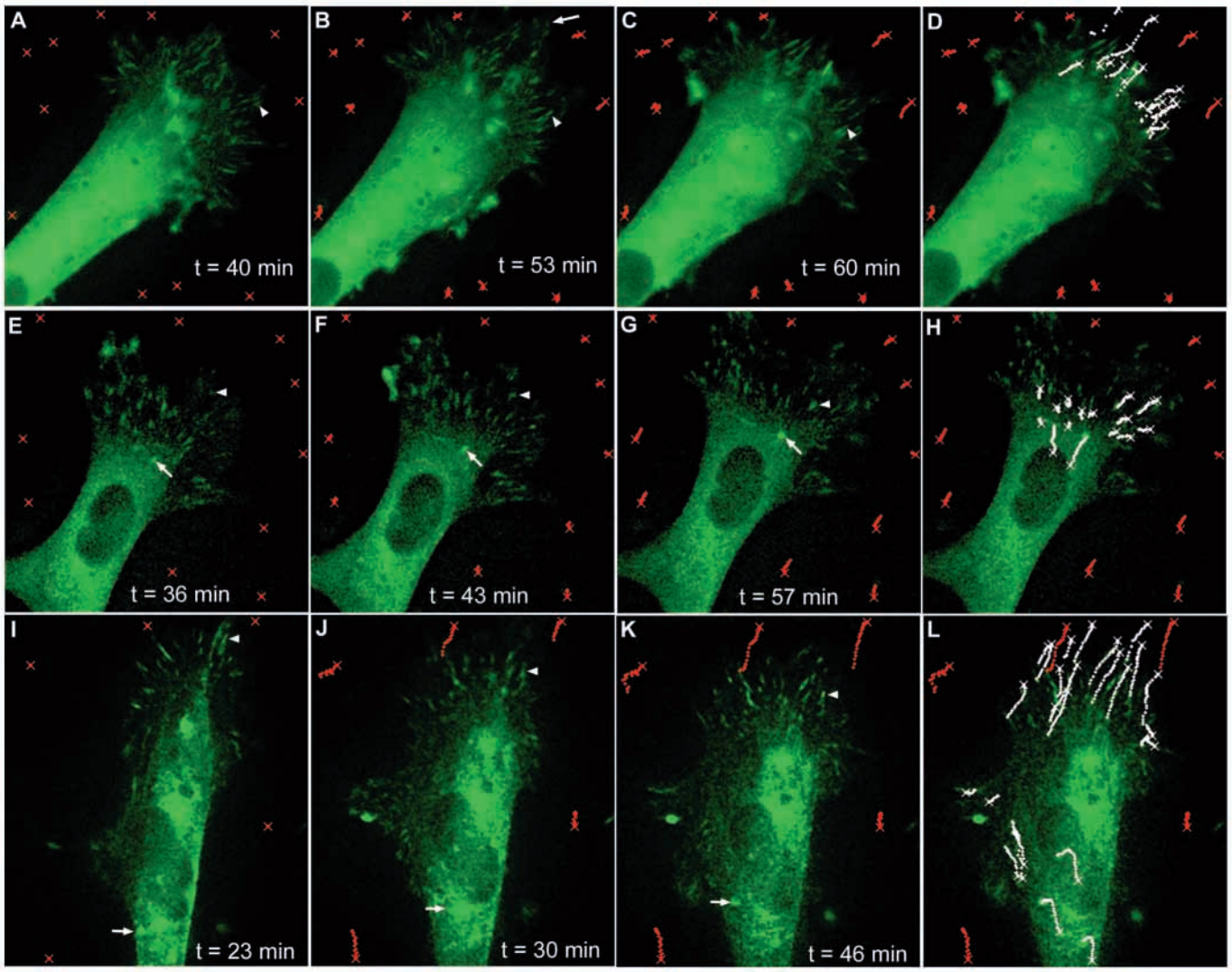

Fig. 4. Comparison of ECM displacements with focal adhesion dynamics in living corneal fibroblasts on top of fibrillar collagen matrices. The red tracks show ECM displacements, whereas the white tracks show adhesion displacements (cross indicates initial position in the sequence). GFP-zyxin images are shown in green. The time (t) is relative to the start of time-lapse imaging. (A-D) The front of a cell moving in a northeast direction. Tracking of the adhesions confirmed our qualitative observation that the adhesions moved inward during cell extension (A-C, arrowheads), and that these movements generally correlated with the ECM deformation in front of the cell (D). See also movie 2 at jcs.biologist.org/supplemental. (E-H) A different cell moving in the northeast direction. Adhesions generally moved perpendicular to the local cell contour, i.e. in a centripetal direction (H), thereby pulling in the ECM in a radial pattern around the front of the cell. Note that as the ECM in front of the cell was pulled backward during extension, the cell body and adjacent ECM was pulled forward, resulting in ECM compression at the base of the lamellipodia. Cell body adhesions (arrows) also moved toward those at the tip (arrowheads), which is consistent with the cell body and ECM movement in this region. (I-L) A cell in which a slow retraction of the lamellipodium was observed. During retraction, adhesions at the front of the cell moved backward in unison (arrowhead) and generated significant ECM deformation. See also movie 3 at jcs.biologist.org/supplemental. At the same time, cell body adhesions moved forward (arrow), resulting in contractile-like shortening of the cell and ECM compression at the base of lamellipodia. See also movies 3 and 4 at jcs.biologist.org/supplemental.

then calculated automatically. This was necessary since adhesions tended to drift in and out of focus over time and could not be tracked using automated procedures. We performed a total of 12 time-lapse experiments using GFP-zyxin. In six of these experiments, tracking of the adhesions was not possible primarily because of too much drift in the focal plane. Nonetheless, these six cells exhibited the same general pattern of adhesion movement and ECM deformation as the cells that were analyzed quantitatively. We measured focal adhesion dynamics during lamellipodial extension at the leading edge in five cells, and partial retraction in one cell. Adhesions were only analyzed in frames in which they were in clear focus.

Tracking of the adhesions confirmed our qualitative observation that the adhesions moved inward during cell extension (Fig. 4A-C, arrowheads), and that these movements generally correlated with the ECM deformation (red tracks) in front of the cell (Fig. 4D; Movie 2, available at jcs.biologists.org/supplemental). Adhesions generally moved perpendicular to the local cell contour, i.e. in a centripetal

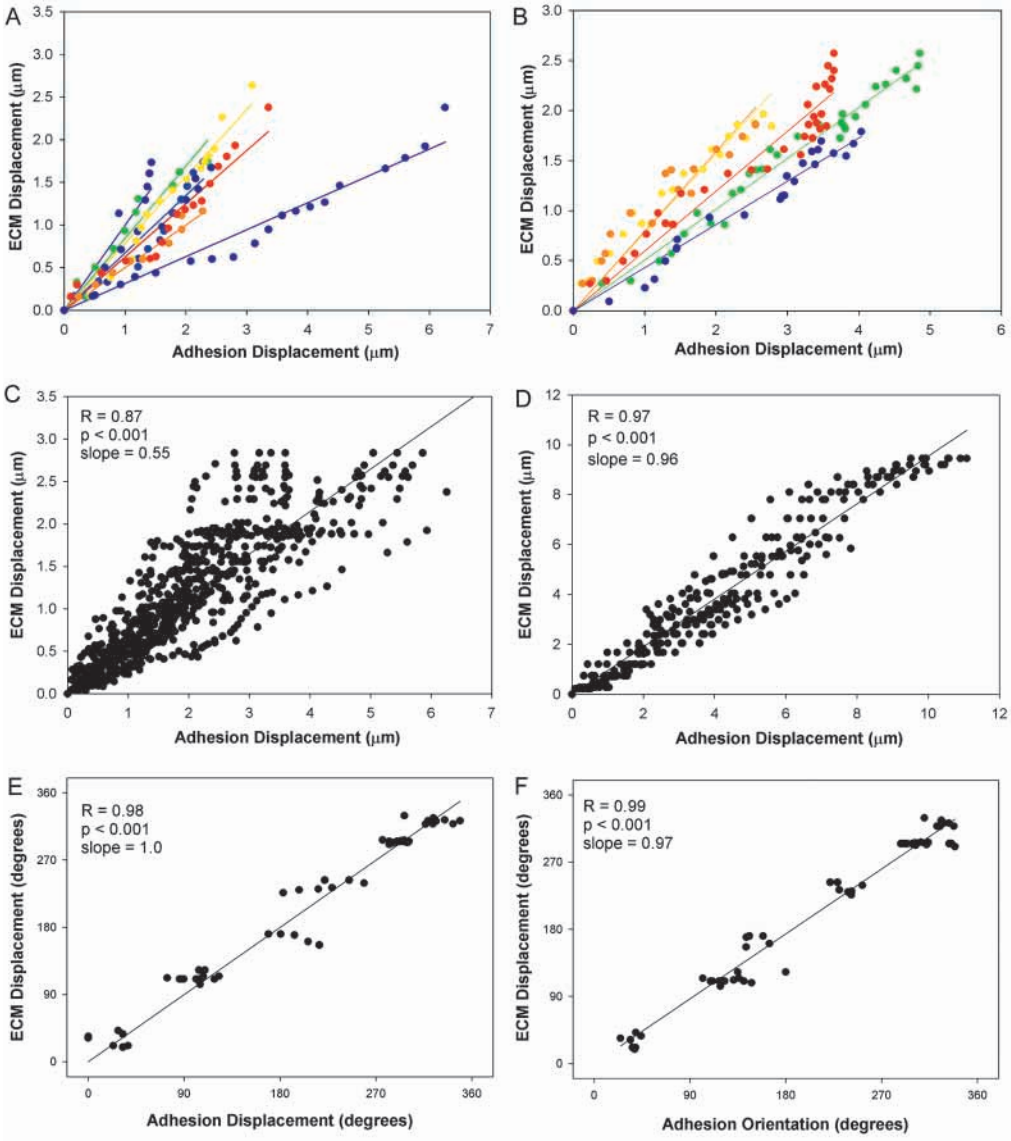

Fig. 5. Quantitative comparison of the magnitude and direction of the movement of adhesions and nearby ECM landmarks. (A,B) Displacement data for two different cells undergoing extension. A significant correlation between adhesion and ECM displacement was found for every adhesion that was tracked (data from each adhesion are shown in a different color). However, the slope of the relationship varied from one adhesion to the next. (C) The pooled data for all five extensions analyzed. A highly significant correlation was found, but the magnitude of adhesion movement was larger than that of the ECM. (D) Data from a cell that underwent slow lamellipodial retraction. A high correlation between the magnitude of ECM and adhesion displacements (R=0.97, P<0.001), and the slope was much closer to 1.0. (E) Comparison of the direction of adhesion and ECM movements for all six experiments combined (five extensions and one retraction). A high correlation was demonstrated, and the slope was 1.0. (F) Since the adhesions tended to assume an oblong shape, we also measured the angle of the long axis of each adhesion (adhesion orientation). The adhesion orientation was highly correlated with the movement of the ECM.

direction (Fig. 4D,H), thereby pulling in the ECM in a radial pattern around the front of the cell.

Interestingly, as the ECM in front of the cell was pulled backward during extension, the cell body and adjacent ECM was pulled forward, resulting in ECM compression at the base of the lamellipodia. In some cases, cell body adhesions were visible in the same focal plane as the lamellipodial adhesions (Fig. 4E-G, arrows); these adhesions always moved toward those at the tip (Fig. 4E-G, arrowheads), consistent with the cell body and ECM movement in this region. This phenomenon was most clearly demonstrated in a cell in which a slow retraction of the front of the cell was observed (Fig. 4I-L). During retraction, adhesions at the front of the cell moved backward in unison (Fig. 4I-K, arrowheads) and generated significant ECM deformation (Movie 3, available at jcs.biologists.org/supplemental). At the same time, cell body adhesions moved forward (Fig. 4I-K, arrows), resulting in contractile-like shortening of the cell and ECM compression at the base of lamellipodia, which is most clearly observed in the DIC time-lapse Movie 4 (available at jcs.biologists.org/supplemental).

In order to quantify the relationship between adhesion displacement and ECM deformation, the magnitude and direction of the movement of adhesions and nearby ECM landmarks were compared. Fig. 5A,B show the displacement data for two different cells undergoing extension. A significant correlation between adhesion and ECM displacement was found for every adhesion that was tracked. However, the slope of the relationship varied from one adhesion to the next

Table 1. Focal adhesion versus ECM displacements

Cell no.	No. of adhesions analyzed	R (mean±s.d.)	P-value (mean)	Slope (mean±s.d.)	Slope (range)
1	9	0.95±0.04	$P \ll 0.001$	0.68±0.21	0.32-1.04
2	7	0.96±0.02	$P \ll 0.001$	0.51±0.07	0.41-0.59
3	14	0.95±0.06	$P \ll 0.001$	0.67±0.23	0.40-1.14
4	7	0.96±0.02	$P \ll 0.001$	0.55±0.17	0.31-0.87
5	5	0.97±0.02	$P \ll 0.001$	0.63±0.17	0.43-0.82
6*	15	0.98±0.01	$P \ll 0.001$	0.95±0.14	0.94-0.99

*This cell underwent partial retraction; whereas cells 1-5 underwent extension.

R, correlation coefficient obtained using linear regression analysis.

(Table 1). The variation in slope was not a function of the distance between the adhesion and DIC landmark, nor was it related to the size of the adhesion or intensity of GFP-zyxin labeling. The pooled data for all five extensions demonstrate a highly significant correlation (R=0.87, $P<0.001$) with a slope of 0.55. Thus in general, the magnitude of adhesion movement was larger than that of the ECM. This could be explained, in part, by the fact that in some regions new adhesions at the leading edge appeared to rupture soon after forming (Fig. 4B, arrow), leading to a rapid and localized retraction of the lamellipodium in this region (Fig. 4C). The movement of the adhesions in these local areas of 'slippage' was usually much greater than that of the nearby ECM. Interestingly, the cell that underwent slow lamellipodial retraction also demonstrated a high correlation between the magnitude of ECM and adhesion displacements (R=0.97, $P<0.001$); however, the slope was much closer to 1.0 (0.96). In general, the pattern of adhesion movement during slow retraction was much less complex than that observed during extension.

During both extension and slow retraction, the directions of adhesion and ECM movements were highly correlated (R=0.98, $P<0.001$; Fig. 5E) and the slope of this relationship was 1.0. Since the adhesions tended to assume an oblong shape, we also measured the angle of the long axis of each adhesion (adhesion orientation). The adhesion orientation was highly correlated with the movement of the ECM (R=0.99, $P<0.001$), suggesting that the adhesions elongate parallel to the direction that they are pulling.

During migration, rupture of adhesions at the tail of the cell was often observed. This led to rapid retraction of a portion of the tail, and release of tension on the ECM. A dramatic example of this is shown in Movie 5 (available at jcs.biologists.org/supplemental). In this case, the rear of the cell completely retracts, and a rapid forward displacement of the cell body (recoil) is observed.

Effects of cell lysis and cytochalasin D treatment

Killing the cells with 1% Triton X-100 resulted in condensation and rounding of cell bodies, complete loss of GFP-zyxin localization, and, in some cases, lifting off of cells from the matrix. ECM relaxation in both the front and rear of the cell was also observed, and there was decompression of the ECM between the cell body and lamellipodium (Movie 6, available at jcs.biologists.org/supplemental). A similar pattern of ECM relaxation was observed within 2-3 minutes after adding cytochalasin D to the media (Fig. 6A,B, red tracks). In some cases the cell body moved forward (Fig. 6), whereas in others it moved backwards, suggesting variable tension in the rear of the cell (Dembo and Wang, 1999). In either case, decompression of the ECM behind the lamellipodium was always observed (Fig. 6, arrows; Movie 7, available at jcs.biologists.org/supplemental). Coincident with this relaxation, the intensity and clarity of the adhesions was significantly reduced, despite attempts to refocus the image. This suggests that there was partial or complete disassembly of the adhesions. However, cells elongated in parallel with the ECM (Movie 7, available at jcs.biologists.org/supplemental), suggesting that some cell-ECM adhesions were still present. The pattern of adhesion formation and inward movement at the leading edge was arrested following treatment with cytochalasin D. When the cytochalasin D was washed out, this pattern of adhesion formation and movement was restored and the ECM was pulled back in (Fig. 6C, yellow tracks).

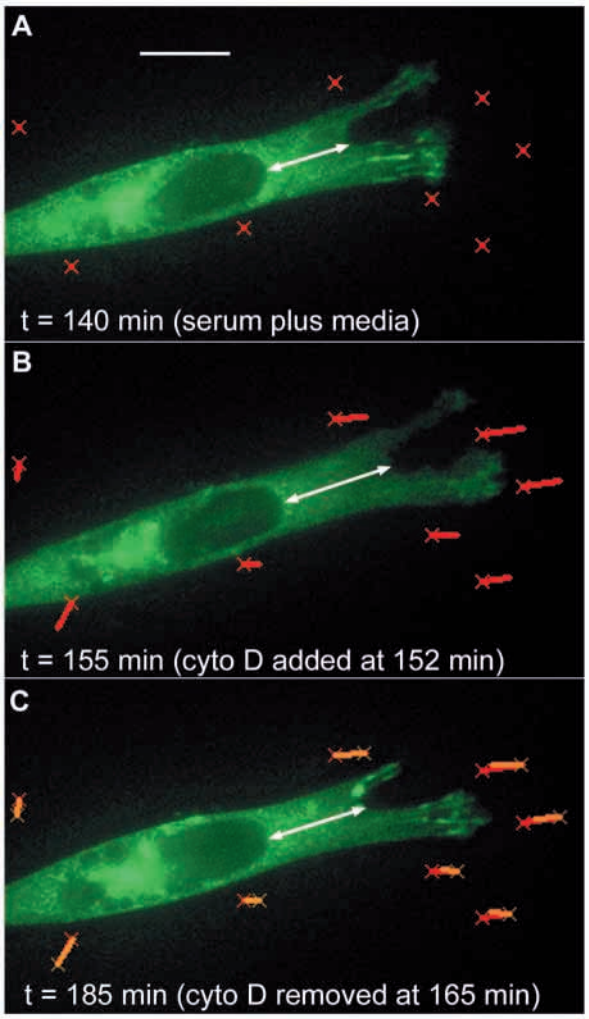

Fig. 6. Effects of cytochalasin D on living corneal fibroblasts plated on top of a fibrillar collagen matrix. The red tracks show ECM displacements, and GFP-zyxin is shown in green. (A) A cell after 140 minutes of time-lapse imaging in complete media. (B) Within three minutes after adding cytochalasin D to the media, cell elongation and ECM relaxation were observed (red tracks). This was most dramatic near the front of the cell. Although the cell body moved forward, decompression of the ECM behind the lamellipodium was still observed (compare length of arrows in A and B). Coincident with ECM relaxation, the intensity and clarity of the adhesions was significantly reduced. (C) After reperfusion with complete media, the adhesions reformed and the ECM was pulled back in (yellow tracks, and arrow). Bar, 10 μm.

Discussion

In this study, we developed and applied a new experimental model for investigating how the organization and movement of cell-matrix adhesion sites correlates with force generation by corneal fibroblasts on a fibrillar collagen extracellular matrix. GFP-zyxin was used to label the adhesion sites, and high magnification time-lapse DIC and fluorescent imaging were

then performed. We found that during lamellipodial extension, new adhesions formed at the leading edge while existing adhesions move backward in a retrograde fashion. Adhesions appeared to disassemble as they reached the base of the extending lamellipodium. This process resulted in ECM displacement that was generally oriented perpendicular to the local cell contour, that is, in a centripetal direction. Both the orientation of the adhesions and the direction of the adhesion displacements were aligned with the ECM displacements in front of the cell. This is consistent with previous observations that focal adhesions are collinear with the direction of force application on the ECM (Balaban et al., 2001). Overall, the data suggest that the centripetal movements of adhesions during lamellipodial extension generate tractional forces that pull in the collagen fibrils in front of the cell.

Interestingly, the cell body and adjacent ECM was pulled forward as the ECM in front of the cell was pulled backward during extension, resulting in ECM compression at the base of the lamellipodia. This compression has been further confirmed by using finite element modeling to generate a strain map of the ECM (W.M.P., unpublished), using a similar but improved approach to that used in previous studies (Roy et al., 1999b). In general, the ventral cell body adhesions were in a focal plane slightly below those at the ends of the cell, and thus were not always visualized. When visible, however, cell body adhesions moved toward those at the leading edge during extension, consistent with the ECM movement in this region. We chose to focus primarily on the leading edge in this study since this is where most of the activity was observed in untransfected control cells. In order to better map the movement of all the focal adhesions in a cell, we are currently investigating whether 3D datasets could be acquired at each time interval without inducing significant phototoxicity or photobleaching.

Overall, the pattern of adhesion movement and ECM displacement we observed at the leading edge of corneal fibroblasts on fibrillar collagen ECM is remarkably similar to the pattern of force generation of migrating NIH 3T3 cells measured by Wang and co-workers (Dembo and Wang, 1999; Munevar et al., 2001a; Munevar et al., 2001b). In their model, collagen coated flexible polyacrylamide sheets embedded with fluorescent microspheres were used as a substratum. A band of intense traction was consistently found within 15 μm of the leading edge of migrating 3T3 cells, as indicated by displacement of the microspheres. These tractions were oriented perpendicular to the local cell contour, i.e. in a centripetal direction. In contrast to the traction at the leading edge of the lamellipodia, the forces at the base of the lamellipodia were oriented in the opposite (centrifugal) direction. Thus an area of compression was produced at a boundary approximately 15 μm behind the leading edge.

On the basis of their data, Wang and co-workers (Munevar et al., 2001a) suggested a ‘frontal towing’ model for cell migration in which the lamellipodium and cell body represent distinct mechanical domains separated by a high shear zone. In this model, adhesions in the lamellipodium transmit strong rearward-directed tractional forces to the substrate. In contrast, adhesions in the rest of the cell serve a more passive anchorage role, and tend to resist forward movement. An ‘elastic transition zone’ corresponding to the region of high shear connects the cell body to the frontal towing zone. The generation and/or transmission of contractile forces in this elastic transition zone provide the forces responsible for towing the cargo.

The focal adhesion data from our study provide important new evidence that supports and extends this frontal towing model of cell motility, and demonstrate for the first time that this mechanism is also used by cells interacting with a fibrillar ECM. In corneal fibroblasts, focal adhesions in the lamellipodia moved rearward as cell body adhesions moved forward, pulling on the ECM and producing an area of compression between them. This is distinctly different from what occurs on rigid substrates, in which focal adhesions are stationary with respect to the substrate, and the cell body moves over them (Smilenov et al., 1999). Interestingly, in one cell, the cell body and its adhesions moved forward at the same time that the leading edge of the cell moved backwards, a phenomenon that cannot be explained by a passive ‘dragging’ mechanism of cell body translocation.

Taken together, the pattern of ECM deformation and focal adhesion displacements suggests that the lamellipodial and cell body adhesions are connected by contractile structures within the elastic transition zone, which may play a central role in generating the forces required for cell migration. Previous studies suggest that these forces are generated via an actin-myosin II based contractile machinery (Chrzanowska-Wodnicka and Burridge, 1996; Jay et al., 1995; Lauffenburger and Horwitz, 1996; Pelham and Wang, 1999; Rottner et al., 1999). Consistent with these results, treatment of corneal fibroblasts with cytochalasin D induced relaxation of the compressed ECM at the base of the lamella, disassembly of adhesions, and elongation of the cells. Cramer et al. (Cramer et al., 1997) recently identified graded polarity actin bundles, in which actin filament polarity gradually changes along the length of the bundle. These structures are oriented parallel to the direction of migration and make up the major population of bundles in locomoting heart fibroblasts. Myosin II is localized to the graded polarity actin bundles, thus it is proposed that these bundles may undergo muscle-like contraction that generates the force needed to pull the cell body adhesions forward and the lamellipodial adhesions backward during locomotion.

We did not attempt to distinguish between different classes of cell-matrix adhesions, since zyxin is a component of both focal complexes (point contacts) and focal adhesions (focal contacts) (Rottner et al., 2001). In general, focal complexes have been associated with lamellipodia and are thought to play a key role in protrusion and traction at the leading edge of migrating cells (Kaverina et al., 2002; Rottner et al., 1999). Focal complexes can either mature into stress fiber-associated focal contacts, or disassemble (turnover) (Webb et al., 2002; Zamir and Geiger, 2001). A recent study comparing the organization of zyxin, vinculin and paxillin during cell migration demonstrated that these proteins are all incorporated into new focal complexes simultaneously, and are also present in focal adhesions (Rottner et al., 2001). Interestingly, zyxin delocalization preceded that of either vinculin or paxillin in adhesions undergoing disassembly.

Although we found a high correlation between the magnitude of adhesion and ECM movements, the slope of this relationship varied from one adhesion to the next. This variation in slope was not a function of the distance between the adhesion and DIC landmarks, nor was it related to the size

of the adhesion or intensity of GFP-zyxin. This finding is not surprising given the variations in adhesion growth, turnover and stability that we observed, and the complex network of actin filaments in the lamella that may provide structural interconnections between adhesions (Cramer et al., 1997; Kaverina et al., 2002; Resch et al., 2002; Small, 1981; Small et al., 1999). Furthermore, the mechanical behavior of an interconnected mesh of collagen fibrils is likely to be more complex than that of a planar elastic substrate (Sawhney and Howard, 2002). One limitation of this study is that ECM displacements were only measured outside of the cell, and therefore reflect the combined contributions of multiple adhesion sites. Measurement of ECM deformation directly under the cell would provide additional insights into the pattern of force generation by adhesions; however, the collagen matrix directly under the cell is difficult to visualize using our current 2D imaging protocol.

The general pattern of adhesion movement and turnover we observed during extension at the leading edge of migrating mammalian corneal fibroblasts on fibrillar collagen matrix is consistent with observations made using fish scale fibroblasts expressing GFP-zyxin on a flexible polyacrylamide substrate (Beningo et al., 2001). It appears that in both cell types the pattern of tractional force generation by adhesions at the leading edge is complex, and is not directly related to the size of the adhesion. In fish scale fibroblasts, small nascent adhesions at the leading edge (i.e. focal complexes) transmitted the largest forces. These adhesions then either disassembled, or matured into larger adhesions; during this maturation, the traction stress transmitted to the matrix by the adhesions decreased. As mentioned above, we were not able to measure the time course of tractional force generation by individual adhesions in this study. However, if new adhesions are mechanically linked to existing adhesions via the actin cytoskeletal network (Matsudaira, 1994; Small, 1981; Small et al., 1999), a reduction in tractional force might be expected as an adhesion moves inward, since a new adhesion at the front of the cell is subjected to only to rearward-directed forces, whereas an adhesion farther back may be pulled in both directions (forward by contractions in front of it, and backwards by contractions behind it). This would place the intracellular domain of the adhesion under progressively more tension as new adhesions formed in front of it, while decreasing the tractional force measured, that is, more of the tension may be absorbed by the cytoskeleton and less transmitted to the ECM.

We found that the organization of the collagen fibrils could be directly visualized using DIC imaging, and we established that landmarks on the DIC images could be used to track ECM deformation. The ability to track ECM deformation directly (i.e. without using beads) will be useful in future studies, since beads degrade the overall quality of the DIC images, use a fluorescent wavelength band that could instead be used for a second fluorescent label, and are sometimes internalized by the cells via endocytosis. In this study, tracking ECM deformation directly from the DIC images in areas where there were no fiduciary beads provided a much more uniform map of the ECM deformation around the cell.

Our new experimental model allows direct, dynamic assessment of cell-ECM interactions on a fibrillar collagen matrix. This approach has important advantages over models using planar elastic substrates. First, cell mechanical interactions on a planar substrate coated with non-fibrillar collagen may be different than that which occurs within a fibrillar extracellular matrix in vivo, since bound, non-fibrillar collagen cannot undergo cell-induced reorganization and remodeling. Furthermore, the collagen fibrils can be directly visualized using DIC imaging, thus cellular reorganization of the collagen matrix can potentially be evaluated. Finally, by mixing cells with the collagen solution prior to polymerization, adhesion dynamics and ECM deformation can potentially be studied in fibroblasts inside the 3D collagen matrices. This is important, since corneal fibroblasts function within a 3D extracellular matrix in vivo. Overall, the continued development and application of this new experimental model should provide important new insights into the underlying mechanisms of cellular force generation and ECM reorganization.

This work was supported by grants from the National Institutes of Health (EY13322), and Research to Prevent Blindness.

References

Balaban, N. Q., Schwarz, U. S., Riveline, D., Goichberg, P., Tzur, G., Sabanay, I., Mahalu, D., Safran, S., Bershadsky, A., Addadi, L. et al. (2001). Force and focal adhesion assembly: a close relationship studied using elastic micropatterned substrates. *Nat. Cell Biol.* **3**, 466-472.

Bell, E., Ivarsson, B. and Merril, C. (1979). Production of a tissue-like structure by contraction of collagen lattices by human fibroblasts of different proliferative potential in vivo. *Proc. Natl. Acad. Sci. USA* **76**, 1274-1278.

Bellows, C. G., Melcher, A. H. and Aubin, J. E. (1981). Contraction and organization of collagen gels by cell cultured from periodontal ligament, ginigiva and bone suggest function cell differences between cell types. *J. Cell Sci.* **50**, 299-314.

Beningo, K. A., Dembo, M., Kaverina, I., Small, J. V. and Wang, Y. L. (2001). Nascent focal adhesions are responsible for the generation of strong propulsive forces in migrating fibroblasts. *J. Cell Biol.* **153**, 881-888.

Chrzanowska-Wodnicka, M. and Burridge, K. (1996). Rho-stimulated contractility drives the formation of stress-fibers and focal adhesions. *J. Cell Biol.* **133**, 1403-1415.

Cramer, L. P., Siebert, M. and Mitchison, T. J. (1997). Identification of novel graded polarity actin filament bundles in locomoting heart fibroblasts: Implications for the generation of motile force. *J. Cell Biol.* **136**, 1287-1305.

Cukierman, E., Pankov, R., Stevens, D. R. and Yamada, K. M. (2001). Taking cell-matrix adhesions to the third dimension. *Science* **294**, 1708-1712.

Dembo, M. and Wang, Y. L. (1999). Stresses at the cell-to-substrate interface during locomotion of fibroblasts. *Biophys. J.* **76**, 2307-2316.

Ehrlich, H. P. (1988). Wound closure: Evidence of cooperation between fibroblasts and collagen matrix. *Eye* **2**, 149-157.

Ehrlich, H. P. and Rajaratnam, J. B. M. (1990). Cell locomotion forces versus cell contraction forces for collagen lattice contraction: an in vitro model of wound contraction. *Tiss. Cell* **22**, 407-417.

Elsdale, T. and Bard, J. (1972). Collagen substrata for studies on cell behavior. *J. Cell Biol.* **54**, 626-637.

Grinnell, F. and Lamke, C. R. (1984). Reorganization of hydrated collagen lattices by human skin fibroblasts. *J. Cell Sci.* **66**, 51-63.

Harris, A. K. (1986). Cell traction in relationship to morphogenesis and malignancy. *Dev. Biol.* **3**, 339-357.

Harris, A. K., Stopak, D. and Wild, P. (1981). Fibroblast traction as a mechanism for collagen morphogenesis. *Nature* **290**, 249-251.

Harris, A. K., Wild, P. and Stopak, D. (1980). Silicone rubber substrata: A new wrinkle in the study of cell locomotion. *Science* **208**, 177-189.

Jay, P. Y., Pham, P. A., Wong, S. A. and Elson, E. L. (1995). A mechanical function of myosin II in cell motility. *J. Cell Sci.* **108**, 387-393.

Kaverina, I., Krylyshkina, O., Gimona, M., Beningo, K., Wang, Y. L. and Small, J. V. (2000). Enforced polarisation and locomotion of fibroblasts lacking microtubules. *Curr. Biol.* **10**, 739-742.

Kaverina, I., Krylyshkina, O. and Small, J. V. (1999). Microtubule targeting of substrate contacts promotes their relaxation and dissociation. *J. Cell Biol.* **146**, 1033-1044.

Kaverina, I., Krylyshkina, O. and Small, J. V. (2002). Regulation of substrate adhesion dynamics during cell motility. *Int. J. Biochem. Cell. Biol.* **34**, 746-761.

Lauffenburger, D. A. and Horwitz, A. F. (1996). Cell migration: A physically integrated molecular process. *Cell* **84**, 359-369.

Lee, J., Leonard, M., Oliver, T., Ishihara, A. and Jacobson, K. (1994). Traction forces generated by locomoting keratocytes. *J. Cell Biol.* **127**, 1957-1964.

Matsudaira, P. (1994). Actin crosslinking proteins at the leading edge. *Semin. Cell Biol.* **5**, 165-174.

Moller-Pedersen, T., Cavanagh, H. D., Petroll, W. M. and Jester, J. V. (1998a). Corneal haze development after PRK is regulated by volume of stromal tissue removal. *Cornea* **17**, 627-639.

Moller-Pedersen, T., Li, H. F., Petroll, W. M., Cavanagh, H. D. and Jester, J. V. (1998b). Confocal microscopic characterization of wound repair after photorefractive keratectomy. *Invest. Ophthalmol. Vis. Sci.* **39**, 487-501.

Munevar, S., Wang, Y. and Dembo, M. (2001a). Traction force microscopy of migrating normal and H-ras transformed 3T3 fibroblasts. *Biophys. J.* **80**, 1744-1757.

Munevar, S., Wang, Y. L. and Dembo, M. (2001b). Distinct Roles of frontal and rear cell-substrate adhesions in fibroblast migration. *Mol. Biol. Cell* **12**, 3947-3954.

Oliver, T., Dembo, M. and Jacobson, K. (1995). Traction forces in locomoting cells. *Cell Motil. Cytoskeleton* **31**, 225-240.

Pelham, R. J., Jr and Wang, Y. (1997). Cell locomotion and focal adhesions are regulated by substrate flexibility. *Proc. Natl. Acad. Sci. USA* **94**, 13661-13665.

Pelham, R. J. and Wang, Y. (1999). High resolution detection of mechanical forces exerted by locomoting fibroblasts on the substrate. *Mol. Biol. Cell* **10**, 935-945.

Petroll, W. M., Cavanagh, H. D., Barry-Lane, P., Andrews, P. and Jester, J. V. (1993). Quantitative analysis of stress fiber orientation during corneal wound contraction. *J. Cell Sci.* **104**, 353-363.

Resch, G. P., Goldie, K. N., Krebs, A., Hoenger, A. and Small, J. V. (2002). Visualization of the actin cytoskeleton by cryo-electron microscopy. *J. Cell Sci.* **115**, 1877-1882.

Rottner, K., Hall, A. and Small, J. V. (1999). Interplay between Rac and Rho in the control of substrate contact dynamics. *Curr. Biol.* **9**, 640-648.

Rottner, K., Krause, M., Gimona, M., Small, J. V. and Wehland, J. (2001). Zyxin is not colocalized with vasodilator-stimulated phosphoprotein (VASP) at lamellipodial tips and exhibits different dynamics to vinculin, paxillin, and VASP in focal adhesions. *Mol. Biol. Cell* **12**, 3103-3113.

Roy, P., Petroll, W. M., Cavanagh, H. D., Chuong, C. J. and Jester, J. V. (1997). An in vitro force measurement assay to study the early mechanical interaction between corneal fibroblasts and collagen matrix. *Exp. Cell Res.* **232**, 106-117.

Roy, P., Petroll, W. M., Cavanagh, H. D. and Jester, J. V. (1999a). Exertion of tractional force requires the coordinated upregulation of cell contractility and adhesion. *Cell Motil. Cytoskeleton* **43**, 23-34.

Roy, P., Petroll, W. M., Chuong, C. J. and Jester, J. V. (1999b). Effect of cell migration on the maintenance of tension on collagen matrix. *Annals Biomed Eng.* **27**, 721-730.

Sawhney, R. K. and Howard, J. (2002). Slow local movements of collagen fibers by fibroblasts drive the rapid global self-organization of collagen gels. *J. Cell Biol.* **157**, 1083-1091.

Small, J. V. (1981). Organization of actin in the leading edge of cultured cells: influence of osmium tetroxide and dehydration on the ultrastructure of actin meshworks. *J. Cell Biol.* **91**, 695-705.

Small, J. V., Rottner, K. and Kaverina, I. (1999). Functional design in the actin cytoskeleton. *Curr. Opin. Cell Biol.* **11**, 54-60.

Smilenov, L. B., Mikhailov, A., Pelham, R. J., Marcatonio, E. E. and Gundersen, G. G. (1999). Focal adhesion motility revealed in stationary fibroblasts. *Science* **286**, 1172-1174.

Stopak, D. and Harris, A. K. (1982). Connective tissue morphogenesis by fibroblast traction. *Dev. Biol.* **90**, 383-398.

Wang, Y. L. and Pelham, R. J., Jr (1998). Preparation of a flexible, porous polyacrylamide substrate for mechanical studies of cultured cells. *Methods Enzymol.* **298**, 489-496.

Webb, D. J., Parsons, J. T. and Horwitz, A. F. (2002). Adhesion assembly, disassembly and turnover in migrating cells – over and over and over again. *Nat. Cell Biol.* **4**, E97-E100.

Zamir, E. and Geiger, B. (2001). Molecular complexity and dynamics of cell-matrix adhesions. *J. Cell Sci.* **114**, 3583-3590.